Separation and Purification Technology 277 (2021) 119484

Contents lists available at ScienceDirect

Separation and Purification Technology

journal homepage: www.elsevier.com/locate/seppur

Customized facilitated transport membranes by mixed strategy for ethylene/ethane separation

Mi Xu [1], Bin Jiang [1], Haozhen Dou, Na Yang, Xiaoming Xiao, Xiaowei Tantai, Yongli Sun, Luhong Zhang [*]

School of Chemical Engineering and Technology, Tianjin University, Tianjin 300072, China

ARTICLE INFO

Keywords:
Gas separation
Facilitated transport membrane
Mixed strategy
Ionic liquid
Solubility and diffusion

ABSTRACT

Mixed strategy has been widely utilized to design novel membranes or tailor membrane structure, however the construction of facilitated transport membranes (FTMs) with mixed strategy has rarely been reported. In this work, eight kinds of mixed protic ionic liquid (MPIL) derived FTMs (MPIL-FTMs) were designed with mixed strategy for highly efficient ethylene/ethane separation by impregnating MPILs and ethylene transport carrier into porous support. The morphology of MPIL-FTMs were characterized by SEM and AFM, and their molecular interactions were investigated by ^{1}H NMR, FTIR and DSC. The MPIL-FTMs exhibited long-term stability and various ethylene permeability-ethylene/ethane selectivity combinations, which indicated mixed strategy could easily customize the separation performances of MPIL-FTMs. Moreover, a fundamental law for mixed strategy was obtained that the two parent PILs with similar chemical structure and molecular interactions favored the synchronous improvement of C_2H_4 permeability and C_2H_4/C_2H_6 selectivity. For example, the C_2H_4 permeability of the [BA][Pyr][NO_3] derived MPIL-FTM reached up to 561.0 Barrer with improved C_2H_4/C_2H_6 selectivity of 26.7, which were superior to most of reported membranes, thus breaking through the ubiquitous trade-off effect. This study proves the mixed strategy is a promising platform for the design of high-performance FTMs as well as their structure modification, and the marriage of mixed strategy with diversity of ILs creates enormous opportunities to construct advanced membranes for energy-intensive gas separations.

1. Introduction

Gas separations are the most important processes in chemical industry,[1] which heavily rely upon distillation, adsorption, extraction, and crystallization.[2,3] However, these traditional separation processes are energy-intensive and account for nearly 15% of the global energy demand, causing serious energy and environmental stress.[4,5] Inspired by specifically and reversibly facilitated transport of small molecules via carrier protein within cell membranes,[6] facilitated transport membranes (FTMs) are fabricated by incorporation of vehicle-like carriers within the membrane matrix, which intelligently integrate the facilitated transport concept with the inherent merits of membrane technology such as less energy supply, small footprint, cost effective and environment-friendly.[7] FTMs continually arouse intensive research interests due to their self-update by extension of application scenarios or combination with novel matrixes such as 2D nanosheets,[8–10] metal/covalent organic frameworks,[11] polyelectrolyte,[12,13] deep eutectic solvent or ionic liquids (ILs).[14–17] And carriers can selectively bind and fast transport the target gas species via the motion of the carrier-target molecule complex (mobile carrier)[18] or the hopping of the species from one carrier to another (fixed carrier).[19] Compared with solid membranes, IL derived FTMs with mobile carriers are featured with higher permeability, easier fabrication of defect-free membranes by spin-coating or pressure-assisted impregnation, high stability and tunable membrane structure.[18,20] All these can be attributed to the advantages of ILs such as faster transport of gas molecules, structural designability, negligible vapor pressure, excellent chemical and thermal stability, which endows FTMs with great potential for various applications such as CO_2 or CO capture,[21–23] O2 enrichment,[24] as well as high-value volatile hydrocarbon purification from natural gas.[25,26]

Mixed strategy or blend strategy is a recognized and effective strategy to directly and precisely tailor the membrane structure and the

* Corresponding author.
E-mail address: zhanglvh@tju.edu.cn (L. Zhang).
[1] M. Xu and B. Jiang, contributed equally.

https://doi.org/10.1016/j.seppur.2021.119484
Received 8 June 2021; Received in revised form 1 August 2021; Accepted 11 August 2021
Available online 19 August 2021

corresponding separation performances, which are associated with the content, molecular weight, chemical structure, compatibility and molecular interactions of two parent matrixes.[27–29] Blended polymer membrane, as the most typical representative of membrane designed by blend strategy, is constructed by blending one polymer matrix with another polymer matrix, which not only enables synergy of two parent polymers but also foster new functionalities. For example, Zhang et al. adopted blend strategy to construct PIM-1/PEG blended membranes with adjustable microstructure, which easily combined the ultrahigh CO_2 permeability of PIM-1 and the excellent CO_2 selectivity of PEG for enhanced CO_2 separation.[30] Scholes et al. fabricated blended polymer membranes with two perfluoro-polymers, and their different solvability in the solvent conferred the blended membranes with miscible or immiscible morphologies, which precisely tuned the CO_2/CH_4 separation performance.[31] By virtue of strong molecular interactions, Wang et al. reported PIM-1/Tröger's Base blended membranes with enhanced CO_2 selectivity and excellent anti-plasticization.[32] Compared with macromolecular polymer, the membrane matrixes with small molecular weight are easier to access the intimate molecular-level mixing, which significantly remold membrane structure.[33,34] ILs act as designable membrane matrixes with small molecular weights, and IL mixtures designed by mixed strategy create enormous capability of subtly tailoring the membrane structure for specific separations benefiting from the unlimited combinations that arise from mixing two or more ILs.[35,36] However, the application of mixed strategy for manipulating the separation performances of IL derived FTMs is rarely reported,[37,38] and very little information is available about how the structure of two selected ILs impacts the properties of the resultant membranes, let alone the corresponding gas solubility and diffusion through the membranes.

Herein, for the first time, we reported the utilization of mixed strategy to construct mixed protic ionic liquid derived FTMs (MPIL-FTMs) as well as precisely tailor membrane structure for highly efficient ethylene/ethane separation. Ethylene/ethane separation acts as the typical example of energy-intensive gas separation and a highly challenging separation due to their similar volatility and molecular size, which is commonly accomplished by cryogenic distillation. The implement of MPIL-FTMs for ethylene/ethane separation generates grand energy-saving and environmental benefits.[39,40] Among all the previously developed membranes for ethylene/ethane separation,[41–43] the FTMs are still the mainstream and exhibit higher separation selectivity due to fast transport of ethylene molecules via carrier, especially for IL derived FTMs.[44,45] Very recently, several groups such as Zhang's group and Ortiz' group are dedicated to the development of IL derived FTMs via molecular design for olefin/paraffin separation,[46–48] and high performance with long-term stability are obtained, which confirms the promising prospect.[49–51] Base on above analysis, eight kinds of MPIL-FTMs were constructed by impregnation of mixed protic ionic liquids into commercial PVDF support, where the membrane morphology and molecular interactions between two different PILs were characterized. The ethylene and ethane permeability, solubility and diffusivity of as-prepared MPIL-FTMs were obtained through permeation and absorption experiments, which were interpreted on the basis of the chemical structure of the selected PILs. It was found that the mixed strategy easily and accurately regulated the gas permeability and separation selectivity, and the synchronous improvement of ethylene permeability and ethylene/ethane selectivity could be achieved by selecting PILs with similar molecular sizes and intermolecular forces. Moreover, the effect of operating conditions and the stability of the MPIL-FTMs were studied systematically, their excellent performances were highlighted by comparison with previously reported membranes.

2. Experimental

2.1. Materials

Ethylene (C_2H_4) and ethane (C_2H_6) with a minimum purity of 99.5% were purchased from Tianjin Tang Dynasty Gas Co., LTD (China). Nitrogen gas (N_2, 5 N) was sourced by Tianjin Dongxiang Gas Co., LTD (China). 3-aminopropanol (99.0%), 2-methoxyethylamine (99.0%), 3-methoxypropylamine (99.0%), 2-(2-aminoethoxy) ethanol (99.0%), pyrrolidine (99.0%), butylamine (99.5%), and silver nitrate ($AgNO_3$) (99.0%) were all supplied by Shanghai Aladdin Biochem Technology Co., Ltd. (China). Nitric acid (65–68%) and methanol were purchased from Tianjin Kermel Chemical Reagent Co., Ltd. (China). All chemicals were used without further purification and the physical and chemical properties of all chemicals were displayed in Table S1 in the Supporting Information. The hydrophilic PVDF support membrane with a porosity of 75%, a pore size of 0.1 μm, an average thickness of 100 μm, and an effective area of 19.625 cm^2 was kindly offered by Haining Zhongli Filtering equipment Corporation (China).

2.2. Synthesis of MPILs

Protic ionic liquids (PILs) were selected as parent membrane matrixes for mixing due to their low-cost, easy fabrication, high polarity and good ability to stabilize ethylene transport carrier. The PILs were prepared by proton transfer reaction based on a similar procedure reported in the literature,[52] and their chemical structure and abbreviations are shown in Fig. 1. In a typical synthesis, a certain amount of aqueous of nitric acid was drop slowly into 3-aminopropanol in a methanol solution at 0 °C or below with rapid stirring. Subsequently, the reaction was carried out at room temperature for 12 h, followed by rotary evaporation to remove water and methanol and drying in vacuum at 80 °C to obtain colorlessness and transparent PIL. Six kinds of PILs were obtained and the MPILs were prepared by mixing two kinds of PILs with different cations at the molar ratio of 1:1. The water contents of the MPILs were measured by Karl – Fischer titration method (DL37 KF Coulometer, Mettler Toledo) and were less than 1.0% by weight.

2.3. Membrane fabrication

MPIL-FTMs were fabricated by the pressure-assistant impregnation method. Initially, $AgNO_3$ was dissolved in the MPILs under magnetic

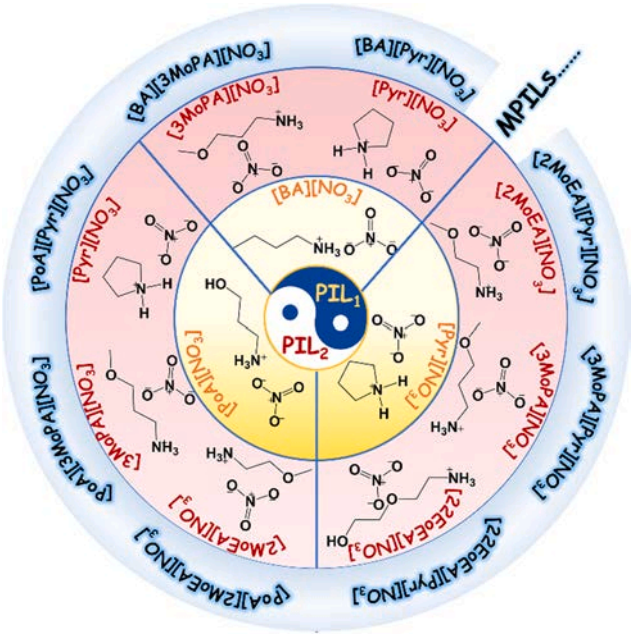

Fig. 1. The chemical structure and abbreviations of MPILs and their parent PILs, where the outermost circle shows the abbreviations of the eight kinds of MPILs, and the corresponding pink and yellow inner circles show the chemical structures and abbreviations of the two parent PILs.

stirring at 60 °C for 3 h, and homogeneous transparent membrane liquids with $AgNO_3$ molar concentration of 2.5 mol/L were obtained for subsequent membrane fabrication. The PVDF support and the membrane liquid were dried at 60 °C for 3 h under vacuum prior to use, and then 3 mL membrane liquid was uniformly coated on the support surface, and intruded into the support pores under the driving force of 1 bar until a visible thin layer of liquid appears at the down surface of the membrane. When the impregnation was completed, the membrane surface was wiped by tissue to remove excess membrane liquid.

2.4. Characterization

Fourier transform infrared (FTIR) spectra were recorded by Bio-Rad FTS-6000 Fourier transform infrared spectrometer at a resolution of 4 cm^{-1} with 32 scans. The ^1H NMR spectra were carried out using a Bruker Avance 500 (500 MHz) spectrometer with DMSO-d_6 as the solvent and tetramethylsilane as the internal standard. The thermal properties were determined by a Q2000 differential scanning calorimetry (DSC) by heating the samples from −140 °C to 20 °C at a heating rate of 5 °C/min in N_2 atmosphere, and the thermal stability was studied using a Netzsch TG 209 thermogravimetric analyzer by heating the samples from RT to 600 °C with a heating rate of 10 °C/min under N_2 atmosphere. The membrane morphology was investigated by field-emission scanning electron microscope (SEM, Hitachi S-4800) and atomic force microscopy (AFM Multimode 8, Bruker, Germany) and the corresponding elemental composition of membranes was obtained by energy dispersive spectrometry (EDS). The AFM images were recorded in the peak-force tapping mode and the average surface roughness (Ra) was determined on the surface area of 10 × 10 μm^2 by Nanoscope image processing software.

2.5. Gas permeation experiment

The mixed-gas permeation experiments were carried out on an apparatus with the schematic diagram shown in Fig. 2. The apparatus is made of stainless steel (AISI 316L) consisting of two feed buffer tanks, a static mixer and a permeation cell which is placed in an air blowing thermostatic oven to control the operating temperature. Before mixed-gas permeation experiments, gas tightness of the whole apparatus was ensured under a constant pressure of 2 bar for 1 h. The MPIL-FTM was fixed in the permeation cell, and C_2H_4/C_2H_6 mixed-gas with molar ratio of 1:1 at a total flow rate of 60 mL/min (STP) flowed directly into the feed side of the permeation cell, while N_2 as a sweep gas entered the permeate side at a flow rate of 20 mL/min (STP). The flow rate was adjusted by mass flow controllers with accuracy of ± 0.5% and the pressure difference between the feed side and the permeate side was recorded by a pressure transducer. The concentrations of C_2H_4 and C_2H_6 in the permeate flow were detected using a on line gas chromatography (Model GC 2008B, Lunan) and the data were continuously recorded every 10 min using a PC until a steady-state condition.

The separation selectivity and the gas permeability through the MPIL-FTMs could be calculated by Eqs. (1) and (2): [15,53]

$$\alpha_{i,j} = \frac{P_{m,i}}{P_{m,j}} \tag{1}$$

$$P_{m,i} = J_i \times \frac{\delta}{\Delta P_i} \tag{2}$$

where $\alpha_{i,j}$ denotes the selectivity, $P_{m,i}$ and $P_{m,j}$ represent the gas permeability of the component *i* and component *j*. J_i is the gas flux of the component *i* through the membrane. δ and ΔP_i is the thickness of the membrane and the transmembrane pressure difference of the component *i*, respectively.

The standard deviation σ of the permeability data was defined as Eqs. (3) :[14]

$$\sigma = \sqrt{\frac{\sum_{t=1}^{n}\left(P_{m,t} - P'_m\right)^2}{n}} \tag{3}$$

where $P_{m,t}$ represents the individual permeability data point of the permeability and P'_m denotes the average of the data. *n* is the number of the measurements. The standard deviation of all test results was less than 0.05, indicating high experimental accuracy.

2.6. Gas adsorption-diffusion study

Adsorptions of C_2H_4 and C_2H_6 on MPIL-FTMs were conducted by a volumetric method on home-made apparatus composed of gas equilibrium vessel of 33.35 cm^3 and gas storage vessel of 116.87 cm^3, where the pressures were monitored using pressure transducers with an accuracy of 0.001 bar and the temperature was maintained at 298 K by a constant temperature circulating water bath with an accuracy of ± 0.1 K. In a typical adsorption experiment, the membrane was placed into the equilibrium vessel and the whole system was evacuated by using a vacuum pump. Subsequently, the gas with a desired pressure was introduced into the gas storage vessel, maintained for 30 min to get the predetermined temperature and the pressure was recorded as P_0. A certain amount of gas was fed into the equilibrium vessel by opening the needle valve connecting the two vessels. After that, the valve connecting the two vessels was closed quickly, and the pressure of the gas storage vessel was recorded as P_1. After the adsorption equilibrium was achieved, the pressure of the equilibrium vessel was referred to as P_2. The pure gas adsorption capacity is determined by Eqs. (4) :[54,55]

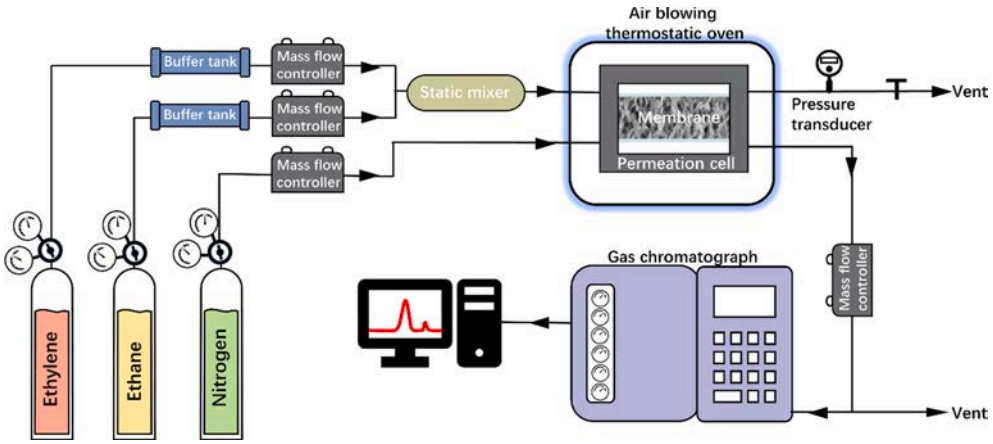

Fig. 2. Diagram of experimental setup.

$$n_i = n_{initial} - n_{final} = \frac{P_0 V_r}{Z_0 RT} - \frac{P_1 (V_s - V_{ml})}{Z_1 RT} - \frac{P_2 V_r}{Z_2 RT} \quad (4)$$

where P_0 is the pressure of the total gas introduced into the gas storage vessel, while P_1 and P_2 are the pressure of equilibration vessel and gas storage vessel at equilibrium. V_r, V_s, and V_{ml} are the volume of the equilibration vessel, gas storage vessel, and the membrane liquid in equilibration vessel, respectively. Z_0, Z_1, and Z_2 are the compressibility factors for the pure gas at different equilibrium states (P_0, P_1 and P_2), which was calculated by Eqs. (5):[56]

$$Z_i = 1 + \frac{P_i B}{RT} (i = 0, 1, 2) \quad (5)$$

where the subscripts of *"0", "1", and "2"* represent different equilibrium states (P_0, P_1 *and* P_2). B is the second-order virial coefficient. The correlation formulas for different gases were illustrated by the Eq. (6) and (7):[52,56]

$$B_{C2H4} = 8.7776 Å \cdot 10\text{-}6.0061 Å \cdot 10^4 / T + 1.2857 Å \cdot 10^6 / T^2 \text{-} 1.0861 Å \cdot 10^9 / T^3 \quad (6)$$

$$B_{C2H6} = 1.0773 Å \cdot 10^2 \text{-} 8.2548 Å \cdot 10^4 / T + 5.2387 Å \cdot 10^6 / T^2 \text{-} 1.9764 Å \cdot 10^9 / T^3 \quad (7)$$

where B_{C2H4} and B_{C2H4} are the second-order virial coefficient of C_2H_4 and C_2H_6, respectively, cm^3/mol, T is the temperature (298.15 K).

The gas transport through MPIL-FTMs was interpreted by the solution-diffusion theory [45,48]. Therefore, the permeability could further be represented as the product of thermodynamic solubility coefficient (S), and kinetic effective diffusion coefficient (D), as shown in Eqs. (8).[57,58]

$$P_i = S_i \bullet D_i \quad (8)$$

The gas solubility coefficient was determined by the gas solubility (n_i), and the effective diffusion coefficient was derived from Equation (8). The permeability selectivity ($\alpha_{i,j}$) was obtained by dividing the permeability of the more permeable specie i to the permeability of the less permeable specie j for the case where the downstream pressure is negligible relative to the upstream feed pressure. As shown in Eqs. (9), the $\alpha_{i,j}$ was also expressed as the product of the diffusivity selectivity and the solubility selectivity. [52]

$$\alpha_{ij} = \frac{P_i}{P_j} = \frac{S_i}{S_j} \bullet \frac{D_i}{D_j} \quad (9)$$

3. Results and discussions

3.1. Structure characterization of MPIL-FTMs

Chemical structure and molecular interactions of MPIL-FTMs were determined by ^{1}H NMR and FTIR spectroscopic characterizations. As seen from the ^{1}H NMR spectra (Fig. 3a), MPILs showed all characteristic chemical shifts of two parent PILs, but with quite different excursion. After the mixing of [BA][NO_3] and [3MoPA][NO_3], all the chemical shifts of C-H groups in MPIL remained at the original position, only one chemical shift of N-H proton was witnessed at 7.838 ppm and slightly shifted to down-field, which were indicative of sufficient mixing at molecular level. In consrtast, all chemical shifts in [PoA][3MoPA][NO_3] MPIL were obviously shifted in relative to [PoA][NO_3] and [3MoPA][NO_3], for exmaple, the chemical shift of O-H significantly moved to down-field from 4.539 ppm to 4.883 ppm (Fig. 3b). Being very different from [BA][3MoPA][NO_3] MPIL, the chemical shifts of N-H proton in [PoA][3MoPA][NO_3] MPIL splited into two different signals at 7.881 ppm and 7.784 ppm. This difference between two MPILs indicated different mixing beviors occurred during mixing two different parent PILs, which were associated with their chemical structures and the variations of molecular interactions during mixing. [BA][NO_3] and [3MoPA][NO_3] had similar molecular sizes and interactions, and the obtained MPIL was probably close to an ideal solution, where the chemical environment of cations and anions and molecular interactions

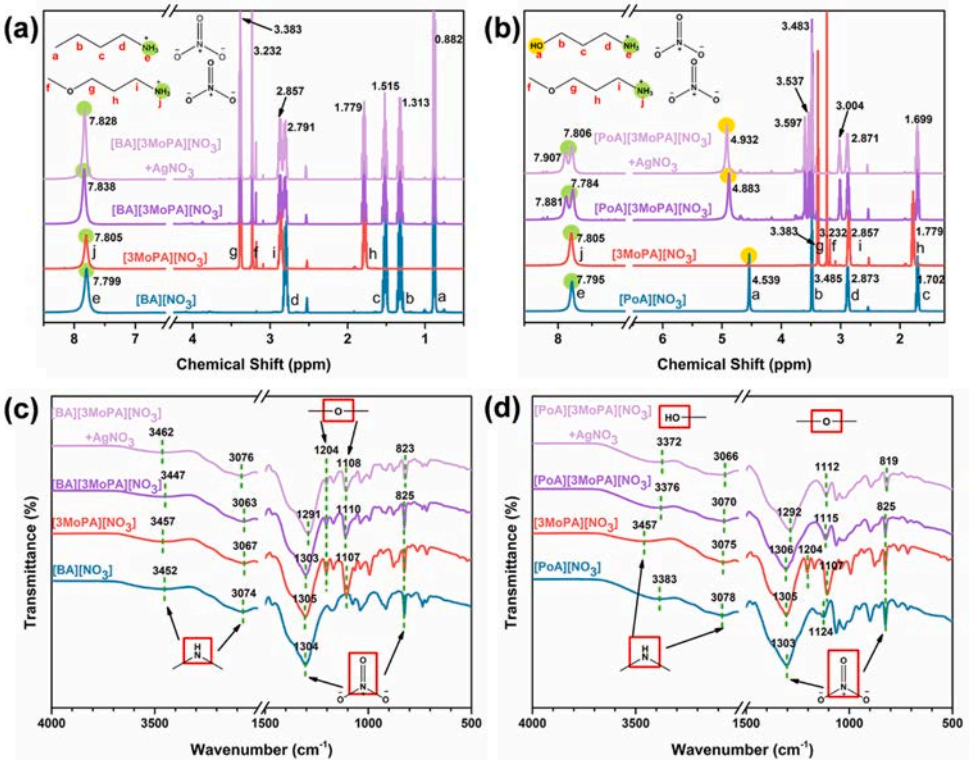

Fig. 3. Chemical structure and molecular interactions characterization of MPIL-FTMs: (a) ^{1}H NMR and (c) FTIR spectra of [BA][3MoPA][NO_3] derived MPIL-FTM, (b) ^{1}H NMR and (d) FTIR spectra of [PoA][3MoPA][NO_3] derived MPIL-FTM.

remained almost unchanged during mixing. However, the molecular sizes and molecular interactions of [PoA][NO_3] and [3MoPA][NO_3] were obviously different, especially considering the high-polarity hydroxyl group in [PoA][NO_3], which meant the strongger hydrogen-bond interactions and self-aggregation. [53] Therefore, the two parent PILs in MPIL maintained part of their respective spatial structures, which were confirmed by two splitted chemical shifts of N-H proton. Meanwhile, some rearrangement of two different PILs spontaneously occurred upon mixing, their different molecular sizes and molecular interactions suggested the chemical environment changed significantly, which resulted in obvious variation of chemical shifts. After the dissolution of silver salt, the chemical shift of N-H proton in [BA][3MoPA][NO_3] MPIL shifted from 7.838 ppm to 7.828 ppm, while the chemical shift of N-H proton in [PoA][3MoPA][NO_3] shifted to down-field from 7.881 ppm and 7.784 ppm to 7.907 ppm and 7.806 ppm, respectively, and the chemical shift of O-H also moved from 4.883 ppm to 4.932 ppm, which indicated the different interactions between MPIL and $AgNO_3$. Therefore, the chemical structures of selected PILs greatly manipulated the structures of resultant MPILs as well as their interactions with ethylene transport carrier.

As seen from Fig. 3c and 3d, few differences in the FTIR spectra of [BA][3MoPA][NO_3] MPIL were observed compared with [BA][NO_3] and [3MoPA][NO_3] owing to their close resemblance in molecular size and chemical structure, which was consitent with ^{1}H NMR reaults. The peaks appeared at around 3447 cm^{-1} and 3063 cm^{-1} were related to the asymmetric stretching vibration and symmetric stretching vibration of –NH-, and the peaks occur at 1303 cm^{-1} and 825 cm^{-1} were assigned as the asymmetric stretching vibration and bending modes of –NO-.[18,59] In addition, the distinct peaks at around 1204 cm^{-1} and 1107 cm^{-1} in [BA][3MoPA][NO_3] MPIL were attributed to the –COC- stretching vibration from the cations of [3MoPA][NO_3].[59] Both the peaks of –NH- vibration and –NO- vibration exhibited red shifts after mixing, which meant the enhancement of the hydrogen bonding interactions and electrostatic interactions. After incorporation of $AgNO_3$ into [BA][3MoPA][NO_3], the –NH- vibration peaks exhibited blue shift to 3462 cm^{-1} and 3076 cm^{-1}, while the –NO- vibration peaks witnessed red shift to 1291 cm^{-1} and 823 cm^{-1}, indicating that hydrogen bonding interactions were reduced but the electrostatic interactions were enchanced. The –COC- stretching vibration also presented red shift slightly from 1110 cm^{-1} to 1108 cm^{-1}, as a confirmation of the interactions between Ag^+ and ether group from [3MoPA][NO_3]. Regarding to the [PoA][3MoPA][NO_3] MPIL, the hydrogen bonding interactions was confirmed by the the broad bands in the –OH stretching region around 3376 cm^{-1}, overinglapping with the –NH- stretching peak around 3457 cm^{-1}, and –NH- stretching at 3070 cm^{-1}. The peaks at 1306 cm^{-1} and 825 cm^{-1} corresponded to the asymmetric stretching vibration and bending modes of –NO- from NO_3^- while 1115 cm^{-1} was associated with the ether bond from the cations of [3MoPA][NO_3]. After addtion of $AgNO_3$ into [PoA][3MoPA][NO_3] MPIL, red shifts of –OH stretching (from 3376 to 3372 cm^{-1}), –NH- symmetric stretching (from 3070 cm^{-1} to 3066 cm^{-1}), –NO- vibration (from 1306 cm^{-1} and 825 cm^{-1} to 1292 cm^{-1} and 819 cm^{-1}) and the –COC- stretching (from 1115 cm^{-1} and 1112 cm^{-1}) were observed due to the reconstruction of hydrogen bonding and electrostatic interactions between [PoA][3MoPA][NO_3] and $AgNO_3$.

The molecular interactions of MPIL-FTMs were further probed by DSC characterization as shown in Fig. 4a. In all samples, only a glass transition temperature (Tg) could be recorded without subsequent cold crystallization and remelting, suggesting the stable liquid state even at very low temperatures. The Tg of [PoA][NO_3] and [3MoPA][NO_3] was −91.24 °C and −96.83 °C, respectivly, while Tg of [PoA][3MoPA][NO_3] MPIL increased significantly to −85.89 °C, which was probably attributed to the denser chain packing and the decrease of flexibility of the cations and anions in MPIL induced by stronger hydrogen bonding interactions.[59] The Tg continued to increase to −78.01 °C as the silver salt was dissolved, which was mainly ascribed to the increase of electrostatic interactions.[7] The TG and DTG curves of [PoA][3MoPA][NO_3] and $AgNO_3$/[PoA][3MoPA][NO_3] were shown in Fig. 4b. The curves displayed one-step weight loss process, which meant the good mixing and the dissolution of carriers in the MPIL. In addition, the thermal decomposition temperatures were higher than 160 °C, confirming satisfactory thermal stability of the resultant MPIL-FTMs.

3.2. Morphology of MPIL-FTMs

The surface and cross-section morphologies of the as-prepared MPIL-FTM were observed by SEM and AFM. Top-view SEM image exhibited the PVDF was a highly porous material with interconnected macropores in the range of 200 nm − 1 μm (Fig. 5a1) and the cross-section image displayed a symmetric three-layered structure with a fiber-penetrating intermediate layer for sufficient mechanical support and a multi-hierarchical distribution of pores (Fig. 5a2 and 5a3). After the impregnation of the $AgNO_3$/MPIL, the pores in the surface were completely saturated by the $AgNO_3$/MPIL due to the presence of capillary forces and a stable layer of $AgNO_3$/MPIL was accumulated on the top surface of the support (Fig. 5b1). The cross-section morphologies of MPIL-FTM indicated the internal pores were homogeneously filled with the $AgNO_3$/MPIL, indicating the good affinity between the $AgNO_3$/MPIL and support (Fig. 5b2 and 5b3). The good affinity and high viscosity of $AgNO_3$/MPIL ensured the as-prepared membrane withstand a certain pressure, which afforded the operational stability of MPIL-FTMs. Therefore, the SEM results confirmed the successful preparation of MPIL-FTMs. The EDS mapping images were recorded to study the elements distribution in the MPIL-FTMs. As observed from Fig. 5c, C, N, O and Ag were almost uniformly distributed, which verified that $AgNO_3$ was well dissolved in the MPIL and the $AgNO_3$/MPIL fulfilled the support pores. The tiny bumps in the EDS images were caused by the accumulation of the mixture on the external surface of the membranes. It was worth

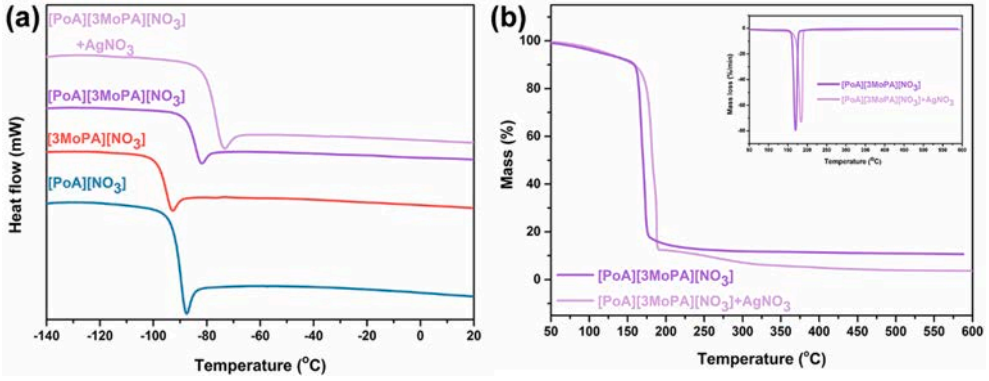

Fig. 4. Thermal stability of MPIL-FTMs. DSC curves (a) and TG curves (b) of [PoA][3MoPA][NO_3] and $AgNO_3$/[PoA][3MoPA][NO_3].

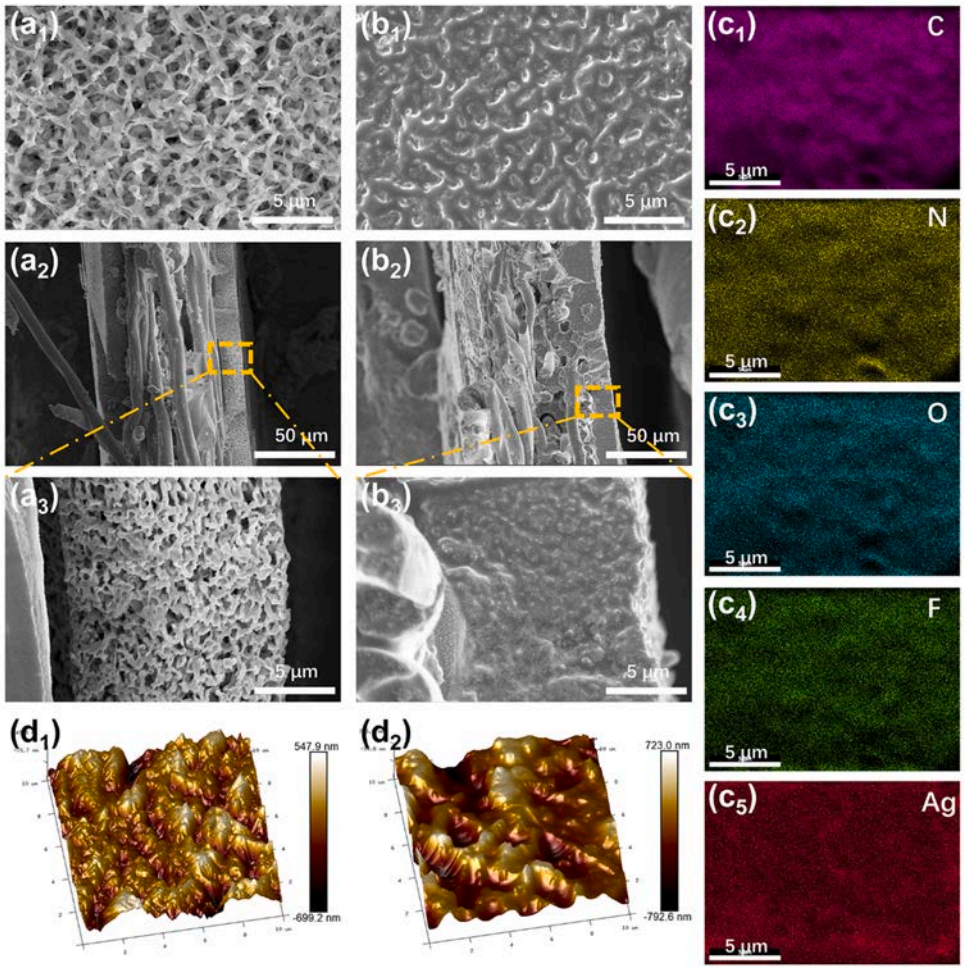

Fig. 5. Membrane morphology study. SEM surface and cross-section images of (a) PVDF support and (b) [PoA][3MoPA][NO_3] derived MPIL-FTM; (c) EDS mapping of [PoA][3MoPA][NO_3] derived MPIL-FTM; (d) AFM images of PVDF support and [PoA][3MoPA][NO_3] derived MPIL-FTM.

mentioning that, the element F from the supporting PVDF could also be detected during elemental analysis, indicating that the $AgNO_3$/MPIL dispersed on the membrane surface was very thin. Furthermore, AFM images were also conducted to investigate the surface morphology and acquire the average surface roughness (Ra) of the MPIL-FTMs (Fig. 5d). In coordination with the result of SEM observations, the roughness of the MPIL-FTM (Ra = 158 nm) was slightly higher than that of pristine PVDF membrane (Ra = 129 nm).

3.3. Separation performance of MPIL-FTMs

Separation performances of MPIL-FTMs for C_2H_4/C_2H_6 mixed gas were evaluated as displayed in Fig. 6. The MPIL-FTMs exhibited various C_2H_4 permeability-C_2H_4/C_2H_6 selectivity combinations, which indicated mixed strategy could easily regulated the separation performances of MPIL-FTMs. According to the change of separation performance of MPIL-FTM in relative to its parent PIL derived FTMs, eight kinds of as-

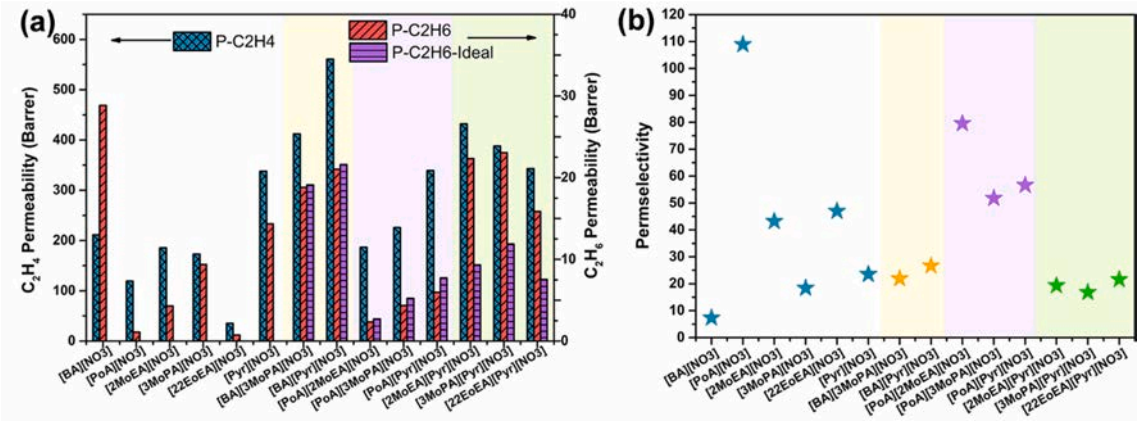

Fig. 6. (a) Gas permeability and (b) C_2H_4/C_2H_6 selectivity of PIL derived FTMs and the resultant MPIL-FTMs.

prepared MPIL-FTMs were classified into three groups: (1) C_2H_4/C_2H_6 selectivity of MPIL-FTM was higher than those of their parent PIL derived FTMs; (2) C_2H_4/C_2H_6 selectivity of MPIL-FTM was located between those of their parent PIL derived FTMs; (3) C_2H_4/C_2H_6 selectivity of MPIL-FTM was lower than that of their parent PIL derived FTMs.

The C_2H_4 permeabilities of [BA][3MoPA][NO_3] and [BA][Pyr][NO_3] derived MPIL-FTMs in first group were much higher than those of their parent PIL derived FTMs, meanwhile C_2H_4/C_2H_6 selectivity was improved simultaneously and the trade-off effect was broken through. For example, the [BA][3MoPA][NO_3] derived MPIL-FTM obtained a C_2H_4 permeability of 412.2 Barrer and C_2H_4/C_2H_6 selectivity of 21.9, which increased significantly compared with the C_2H_4 permeabilities of [BA][NO_3] derived FTM (211.6 Barrer) and [3MoPA][NO_3] derived FTM (172.9 Barrer). As for [BA][Pyr][NO_3] derived MPIL-FTM, the C_2H_4 permeability reached up to 561.0 Barrer with improved C_2H_4/C_2H_6 selectivity of 26.7, which was almost three times of that of [BA][NO_3] derived FTM (211.6 Barrer) and much higher than [Pyr][NO_3] derived FTM (337.8 Barrer). The excellent C_2H_4 permeability may be originate from the enhanced carrier activity and desirable membrane structure. It is well acknowledged that C_2H_6 permeability is mainly occurred via a physically solution-diffusion mechanism. C_2H_6 permeabilities of MPIL-FTMs were very close to the average of those of their parent PIL derived FTMs, the ratios were 0.985 and 0.974 for [BA][3MoPA][NO_3] and [BA][Pyr][NO_3] derived MPIL-FTMs, respectively, which suggested that the ideal mixture probably occurred and C_2H_6 permeability almost followed ideal mixing law. This behavior was attributed to the similar chemical structure and molecular interactions of two selected parent PILs, which was in well agreement with spectroscopic characterizations.

C_2H_4 permeabilities and [PoA][2MoEA][NO_3], [PoA][3MoPA][NO_3] and [PoA][Pyr][NO_3] derived MPIL-FTMs in second group were close to or slight higher than their parent PIL derived FTM with larger C_2H_4 permeability, while their C_2H_4/C_2H_6 selectivity was located between those of their parent PIL derived FTMs. It was found that the C_2H_6 permeability followed a declining trend when compared with the average of the two parent PIL derived FTMs. The ratio of the C_2H_6 permeabilities of MPIL-FTMs to the corresponding averages were 0.87, 0.83 and 0.78, respectively, which was probably attributed to the newly formed molecular interactions during mixing, thus leading to more tightly packed arrangement of cations and anions and more compact membrane structure in relative to ideal mixing. As for third group, C_2H_4 permeabilities of [2MoEA][Pyr][NO_3], [3MoPA][Pyr][NO_3] and [22EoEA][Pyr][NO_3] derived MPIL-FTMs increased sharply and were much higher than those of their parent PIL derived FTMs. Unfortunately, C_2H_4/C_2H_6 selectivity decreased after mixing, for example, the C_2H_4/C_2H_6 selectivity of [3MoPA][Pyr][NO_3] derived MPIL-FTM was only 16.8 and much lower than that of [Pyr][NO_3] derived FTM (23.5). Being different with first group and second group, C_2H_6 permeability of MPIL-FTMs increased very sharply and much higher than the average of C_2H_6 permeabilities of their parent PIL derived FTMs. In third group, the two parent PILs exhibited big difference in chemical structure and molecular interactions, which gave rise to the chaotic and irregularly arrangement of cations and anions during mixing, significantly increasing gas permeability. The much more significant improvement of C_2H_6 permeability in relative to C_2H_4 permeability resulted in the decrease of C_2H_4/C_2H_6 selectivity. By comparison of above-mentioned three groups, a fundamental law for mixed strategy was obtained that the selection of two ILs with similar chemical structure and molecular interactions was the best choice to construct high-performance mixed IL derived FTMs. Similar resulted have been reported by metal organic framework membranes with mixed-chain strategy that the utilization of two organic linkers with similar structure favored the high-performance.[3]

3.4. Gas solubility and diffusivity of MPIL-FTMs

The gas permeation through the MPIL-FTMs was further analyzed by the solubility and diffusivity (Fig. 7). Regardless of PIL derived FTMs and MPIL-FTMs, C_2H_4 solubility was always greater than that of C_2H_6, where the C_2H_4 solubility included physical and chemical solubility while the C_2H_6 solubility only depended on physical solubility. It could be also clearly concluded that C_2H_4/C_2H_6 selectivity was dominated by the solubility selectivity. [19,52] By comparing of MPIL-FTMs with their parent PIL derived FTMs, the effect of mixed strategy on the gas solubility and diffusivity could be obtained, which was further coordinated with the gas permeability and chemical structure of MPIL-FTMs. As for MPIL-FTMs in first group, the C_2H_4 solubility and diffusivity increased after mixing while the C_2H_6 solubility and diffusivity almost remained the same with the average value of the two parent PIL derived FTMs, the synchronous improvement of solubility selectivity and diffusion selectivity resulted the excellent C_2H_4 permeability as well as enhanced C_2H_4/C_2H_6 selectivity. In second group, the C_2H_4 and C_2H_6 solubilities and solubility selectivity of MPIL-FTMs were located between their parent PIL derived FTMs, but the mixed strategy contributed to the increase of diffusivity selectivity. Then it came to third group, the C_2H_4 solubility increased but C_2H_4 diffusivity was located between those of two parent PIL derived FTMs. In contrast, both C_2H_6 solubility and diffusivity increased very sharply due to the severely disordered rearrangement structure, which led to the simultaneous decrease of solubility selectivity and diffusivity selectivity. Based on the above analysis, the mixed strategy generated on important but different effect on both gas solubility and diffusivity, the mixture of PIL with similar chemical structures could promote the C_2H_4/C_2H_6 solubility selectivity and diffusivity selectivity synchronously.

3.5. Effect of operating conditions

The effects of temperature and transmembrane differential pressure on separation performances of MPL-FTMs were investigated by selecting [BA][3MoPA][NO_3] derived MPIL-FTMs as a representative, where the results were presented in Fig. 8. The permeability of C_2H_4 and C_2H_6 increased synchronously with operating temperature because of the molecular interactions were weakened and the viscosity of MPIL decreased at higher temperature, which facilitated the gas diffusivity. [52] However, the complexation reaction between the carrier and C_2H_4 was exothermic and the C_2H_4 solubility decreased more obviously than that of C_2H_6 as the temperature increasing from 25 °C to 65 °C. As a result, a lower C_2H_4/C_2H_6 selectivity was observed (Fig. 8a). As shown in Fig. 8b, the transmembrane differential pressure had almost no effect on the C_2H_6 permeability through the [BA][3MoPA][NO_3] derived MPIL-FTM, which followed the solution-diffusion mechanism. In contrast, the C_2H_4 permeability dropped by 60% from 412.2 Barrer to 165.0 Barrer when the transmembrane differential pressure increased from 0.1 bar to 1.48 bar, which was a common phenomenon within FTMs that the active carrier rapidly reached saturation even at a lower pressure and failed to coordinate with more ethylene molecules at higher temperature.[15] Therefore, the C_2H_4/C_2H_6 selectivity of MPIL-FTMs decreased with the increase of transmembrane differential pressure.

3.6. Stability and comparison

The long-term operational stability of MPIL-FTM was evaluated by the gas permeation experiment. As shown in Fig. 8c, the C_2H_4 permeability, C_2H_6 permeability as well as C_2H_4/C_2H_6 selectivity of the MPIL-FTMs experienced a sharp decline in the first two hours, after which no obvious change was pronounced during the 180-hour operation. This result confirmed excellent long-term stability of the MPIL-FTMs, which was vital for industrial application and economic feasibility. The mass of [PoA][3MoPA][NO_3] based MPIL-FTM before and after long-term stability measurement was also weighed by an electronic balance with accuracy of 0.0001 g. The weight of MPIL-FTM decreased by 14.6 mg after running for 180 h and the mass loss only accounted for about 1.35

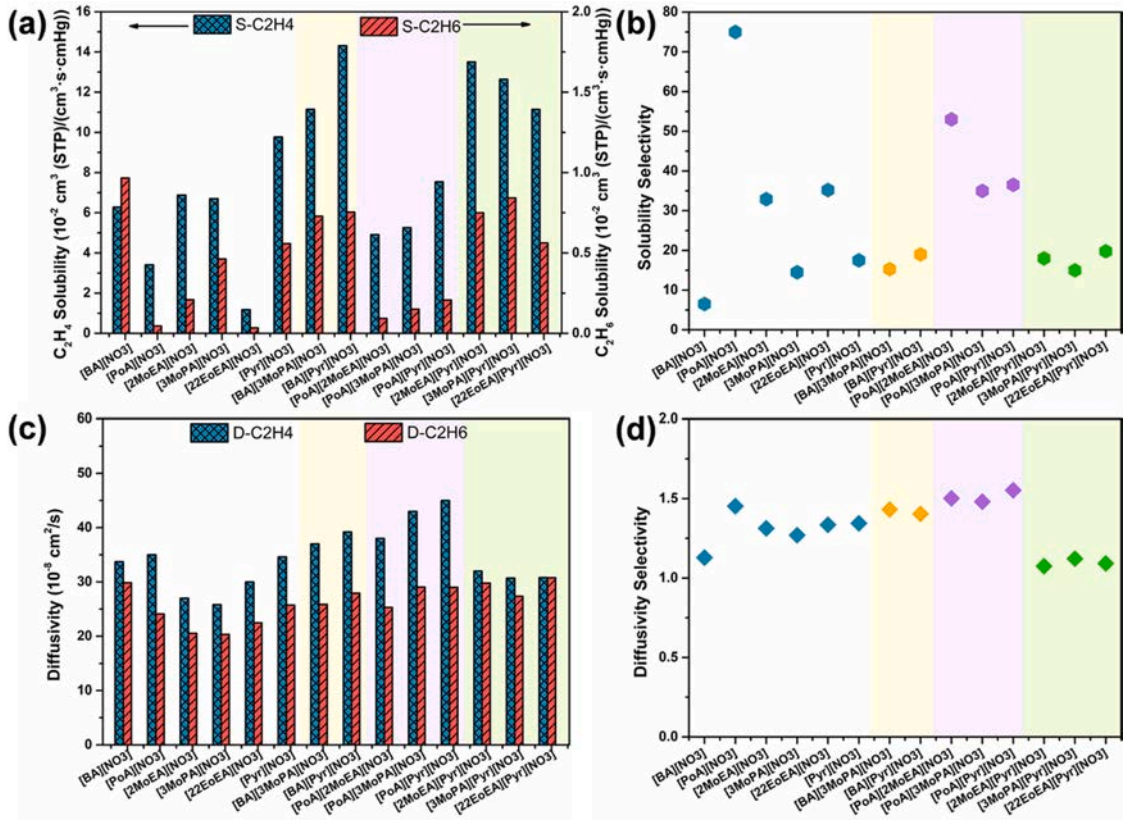

Fig. 7. The gas solubility and diffusivity properties of the MPIL-FTMs. (a) gas solubility, (b) solubility selectivity, (c) gas diffusivity and (d) diffusivity selectivity.

wt% of total weight of MPIL-FTM, which suggested almost no release of MPILs and confirmed the excellent stability of MPIL-FTM. In addition, in order to demonstrate the chemical stability of the as-fabricated MPIL-FTMs, the membranes were exposed to the lab environment without any protection and with H_2 atmosphere respectively for 90 days, and then characterized by FTIR to investigate the stability of the carriers. It is well known that the FTMs often suffer from carrier instability due to photoreduction or reduced by exposition to reductant gases of H_2, and the silver ions within membranes are easily reduced to silver particles. [60] However, it could be found that both the color and FTIR spectra of the MPIL-FTMs remained unchanged (Fig. 8d and 8e), indicating the carriers' stability even under the reductive conditions, which was probably derived from that the silver ions were stabilized by MPILs because of the useful Brönsted acidic property.[52]

Finally, the excellent separation performances of our membrane were highlighted by comparing our membranes with the state-of-the-art membranes for C_2H_4/C_2H_6 separation (Fig. 8f). It should be noted that the mixed strategy could improve the C_2H_4 permeability without sacrificing C_2H_4/C_2H_6 selectivity, and the performance of MPIL-FTMs tremendously surpassed the Robeson upper bound for polymer membrane proposed by Koros in 2013.[61] Especially, the C_2H_4/C_2H_6 selectivity reached up to 79 of the [PoA][2EoEA][NO_3] derived MPIL-FTM, which was very competitive with recently reported IL and DES derived FTMs. Therefore, the above results clearly showed the application potential of the MPIL-FTMs for C_2H_4/C_2H_6 separation.

4. Conclusions

In this study, the facile and straightforward mixed strategy was utilized to design novel IL derived FTMs, which extended the scope of IL derived membrane and proved a promising platform to tailor the membrane performance. A series of MPIL-FTMs were constructed by impregnating the $AgNO_3$/MPIL into the porous PVDF support, which could easily regulate and customize the C_2H_4/C_2H_6 separation performance upon careful selection of parent PILs. The morphology of the resultant MPIL-FTMs was revealed by SEM and AFM, and their molecular interactions were determined by ^{1}H NMR, FTIR and DSC characterizations, as well as their satisfactory thermal stability was verified by TG. The results indicated that the chemical structure of selected PILs greatly manipulated the structures of resultant MPIL-FTMs as well as the interactions between MPIL and ethylene-transport carrier. The gas separation performances of MPIL-FTMs were investigated and divided into three groups depending on their difference compared with their parent PIL derived FTMs, where a fundamental law for mixed strategy was obtained that the selection of two ILs with similar chemical structure and molecular interactions was the best choice to construct high-performance mixed IL based FTMs. The gas solubility and diffusivity of MPIL-FTMs were also investigate and further coordinated with chemical structure of selected PILs, where the PILs with similar chemical structure and molecular interactions favored the synchronous improvement of both gas solubility and diffusivity, thus leading much better performances of MPIL-FTMs than those of their parent PIL derived FTMs. Moreover, MPIL-FTMs exhibited good long-term stability and was competitive with recently reported IL and DES derived FTMs. This study proves that mixed strategy is a simple but powerful tool to create MIL-FTMs with tunable structures and customized performances, which can become the substitution for task-specific IL derived membranes with high-cost and complicated synthesis, and deep insights of the relationship between the separation performances of MPIL-FTMs and the chemical structure of selected parent ILs will shed light on the design of high-performance FTMs for precise molecular separation.

Declaration of Competing Interest

The authors declare that they have no known competing financial interests or personal relationships that could have appeared to influence

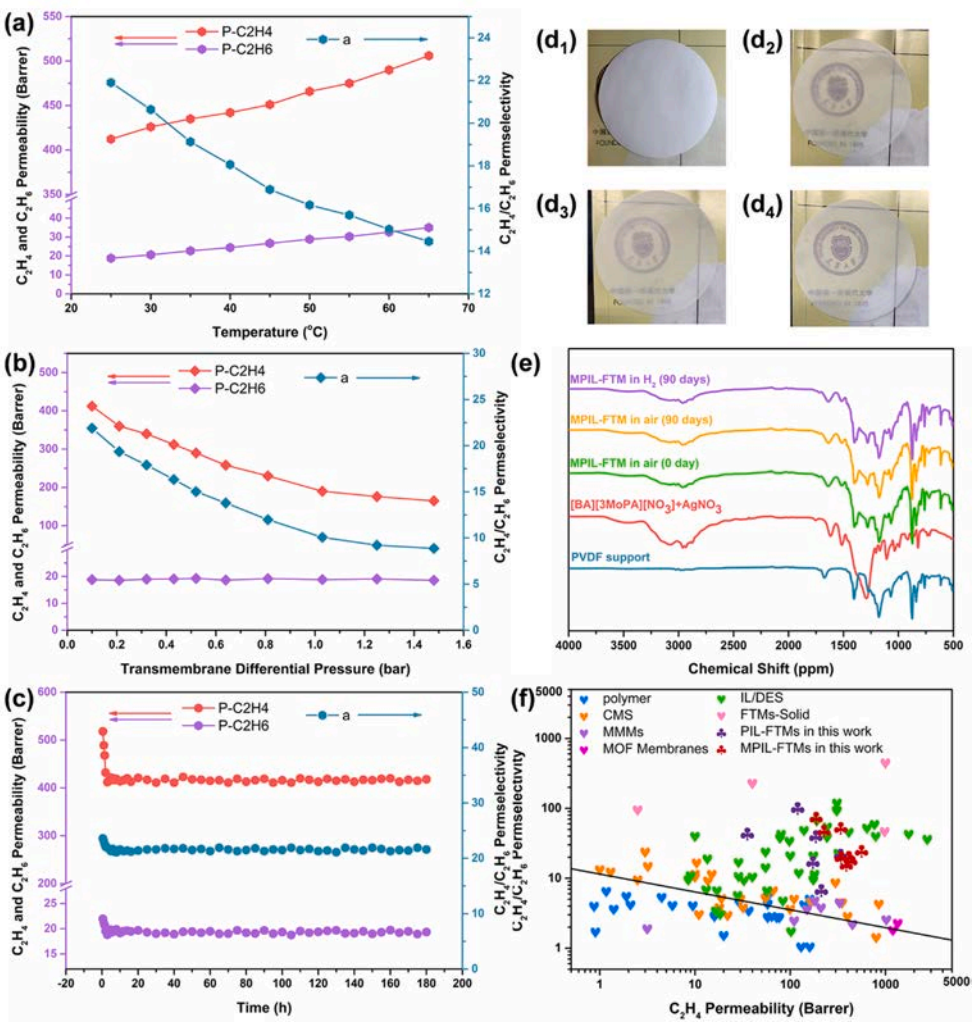

Fig. 8. Operating condition optimization and the evaluation of membrane stability. (a) Effect of operating temperature on separation performance of the MPIL-FTMs; (b) Effect of transmembrane differential pressure on separation performance of the MPIL-FTMs; (c) Long-term operational stability; (d) Optical images of MPIL-FTMs under different atmospheres: (d_1) pure PVDF support membrane, (d_2) freshly-baked MPIL-FTM, (d_3) MPIL-FTM stored in air for 90 days, (d_4) MPIL-FTM stored in H_2 for 90 days; (e) FTIR spectra of MPIL-FTMs; and (f) Highlight of separation performances of MPIL-FTMs by comparison of this study with previous studies. (Note: the MPIL-FTM used here was [PoA][3MoPA][NO_3] derived MPIL-FTM.)

the work reported in this paper.

Acknowledgments

We are grateful for the financial support from National Natural Science Foundation of China (No. 22078233).

Appendix A. Supplementary material

Supplementary data to this article can be found online at https://doi.org/10.1016/j.seppur.2021.119484.

References

[1] J.B. James, J. Wang, L. Meng, Y.S. Lin, ZIF-8 Membrane Ethylene/Ethane Transport Characteristics in Single and Binary Gas Mixtures, Ind. Eng. Chem. Res. 56 (2017) 7567–7575.
[2] S. Yi, B. Ghanem, Y. Liu, I. Pinnau, W.J. Koros, Ultraselective glassy polymer membranes with unprecedented performance for energy-efficient sour gas separation, Science, Advances 5 (2019) eaaw5459.
[3] H. Dou, M. Xu, B. Wang, Z. Zhang, G. Wen, Y. Zheng, D. Luo, L. Zhao, A. Yu, L. Zhang, Z. Jiang, Z. Chen, Microporous framework membranes for precise molecule/ion separations, Chem. Soc. Rev. (2021).
[4] Y. Ren, X. Liang, H. Dou, C. Ye, Z. Guo, J. Wang, Y. Pan, H. Wu, M.D. Guiver, Z. Jiang, Membrane-Based Olefin/Paraffin Separations, Adv. Sci. 7 (2020) 2001398.
[5] S. Chu, Y. Cui, N. Liu, The path towards sustainable energy, Nat. Mater. 16 (2017) 16–22.
[6] Y. Li, S. Wang, G. He, H. Wu, F. Pan, Z. Jiang, Facilitated transport of small molecules and ions for energy-efficient membranes, Chem. Soc. Rev. 44 (2015) 103–118.
[7] H. Dou, M. Xu, B. Wang, Z. Zhang, D. Luo, B. Shi, G. Wen, M. Mousavi, A. Yu, Z. Bai, Z. Jiang, Z. Chen, Analogous mixed matrix membranes with self-assembled interface pathways, Angew. Chem. Int. Ed. n/a (2020).
[8] C.S. Lee, M.-K. Choi, Y.Y. Hwang, H. Kim, M.K. Kim, Y.J. Lee, Facilitated Water Transport through Graphene Oxide Membranes Functionalized with Aquaporin-Mimicking Peptides, Adv. Mater. 30 (2018).
[9] H. Dou, M. Xu, B. Jiang, G. Wen, L. Zhao, B. Wang, A. Yu, Z. Bai, Y. Sun, L. Zhang, Z. Chen, Z. Jiang, Bioinspired Graphene Oxide Membranes with Dual Transport Mechanisms for Precise Molecular Separation, Adv. Funct. Mater. 29 (2019) 1905229.
[10] H. Dou, B. Jiang, M. Xu, Z. Zhang, G. Wen, F. Peng, A. Yu, Z. Bai, Y. Sun, L. Zhang, Boron Nitride Membranes with a Distinct Nanoconfinement Effect for Efficient Ethylene/Ethane Separation, Angewandte Chemie International Edition, (2019).
[11] F. Pan, M. Wang, H. Ding, Y. Song, W. Li, H. Wu, Z. Jiang, B. Wang, X. Cao, Embedding Ag+@COFs within Pebax membrane to confer mass transport channels and facilitated transport sites for elevated desulfurization performance, J. Membr. Sci. 552 (2018) 1–12.
[12] H. Jeon, Y. Cho, S.W. Kang, Structural Effect of Ionic Liquid on Long-Term Stability in Poly(ethylene oxide)/Ag Ions/Ag Nanoparticles Composite for Olefin Separation, Macromol. Res. 28 (2020) 445–449.
[13] K.W. Yoon, Y.S. Kang, S.W. Kang, Activated Ag ions and enhanced gas transport by incorporation of KIT-6 for facilitated olefin transport membranes, J. Membr. Sci. 513 (2016) 95–100.
[14] H. Dou, B. Jiang, L. Zhang, M. Xu, Y. Sun, Synergy of high permeability, selectivity and good stability properties of silver-decorated deep eutectic solvent based facilitated transport membranes for efficient ethylene/ethane separation, J. Membr. Sci. 567 (2018) 39–48.
[15] B. Jiang, J. Zhou, M. Xu, H. Dou, H. Zhang, N. Yang, L. Zhang, Multifunctional ternary deep eutectic solvent-based membranes for the cost-effective ethylene/ethane separation, J. Membr. Sci. 610 (2020), 118243.

[16] B. Jiang, H. Dou, L. Zhang, B. Wang, Y. Sun, H. Yang, Z. Huang, H. Bi, Novel supported liquid membranes based on deep eutectic solvents for olefin-paraffin separation via facilitated transport, J. Membr. Sci. 536 (2017) 123–132.

[17] X. Zhang, W. Xiong, Z. Tu, L. Peng, Y. Wu, X. Hu, Supported Ionic Liquid Membranes with Dual-Site Interaction Mechanism for Efficient Separation of CO2, ACS Sustain. Chem. Eng. 7 (2019) 10792–10799.

[18] H. Dou, M. Xu, B. Wang, Z. Zhang, G. Wen, F. Peng, K. Zarshenas, D. Luo, A. Yu, Z. Bai, Self-assembled Facilitated Transport Membranes with Tunable carrier Distribution for ethylene/ethane Separation, Adv. Funct. Mater. 2104349 (2021).

[19] H. Dou, B. Jiang, M. Xu, J. Zhou, Y. Sun, L. Zhang, Supported ionic liquid membranes with high carrier efficiency via strong hydrogen-bond basicity for the sustainable and effective olefin/paraffin separation, Chem. Eng. Sci. 193 (2019) 27–37.

[20] H. Dou, M. Xu, B. Wang, Z. Zhang, D. Luo, B. Shi, G. Wen, M. Mousavi, A. Yu, Z. Bai, Analogous Mixed Matrix Membranes with Self-Assembled Interface Pathways, Angew. Chem. Int. Ed. 60 (2021) 5864–5870.

[21] G. Zarca, I. Ortiz, A. Urtiaga, Copper(I)-containing supported ionic liquid membranes for carbon monoxide/nitrogen separation, J. Membr. Sci. 438 (2013) 38–45.

[22] Z. Shamair, N. Habib, M.A. Gilani, A.L. Khan, Theoretical and experimental investigation of CO2 separation from CH4 and N2 through supported ionic liquid membranes, Appl. Energy 268 (2020) 115016.

[23] A.S.L. Gouveia, M. Yáñez, V.D. Alves, J. Palomar, C. Moya, D. Gorri, L.C. Tomé, I. M. Marrucho, CO2/H2 separation through poly(ionic liquid)–ionic liquid membranes: The effect of multicomponent gas mixtures, temperature and gas feed pressure, Sep. Purif. Technol. 259 (2021) 118113.

[24] A. Matsuoka, E. Kamio, T. Mochida, H. Matsuyama, Facilitated O2 transport membrane containing Co(II)-salen complex-based ionic liquid as O2 carrier, J. Membr. Sci. 541 (2017) 393–402.

[25] A. Khakpay, P. Scovazzo, S. Nouranian, Homogeneous and biphasic cellulose acetate/room temperature ionic liquid membranes for gas separations: Solvent and phase-inversion casting vs. supported ionic liquid membranes, J. Membr. Sci. 589 (2019) 117228.

[26] Z. Tu, P. Liu, X. Zhang, M. Shi, Z. Zhang, S. Luo, L. Zhang, Y. Wu, X. Hu, Highly-selective separation of CO2 from N2 or CH4 in task-specific ionic liquid membranes: Facilitated transport and salting-out effect, Sep. Purif. Technol. 254 (2021) 117621, https://doi.org/10.1016/j.seppur.2020.117621.

[27] A. Behboudi, Y. Jafarzadeh, R. Yegani, Polyvinyl chloride/polycarbonate blend ultrafiltration membranes for water treatment, J. Membr. Sci. 534 (2017) 18–24.

[28] M. Klepić, K. Setničková, M. Lanč, M. Žák, P. Izák, M. Dendisová, A. Fuoco, J. C. Jansen, K. Friess, Permeation and sorption properties of CO2-selective blend membranes based on polyvinyl alcohol (PVA) and 1-ethyl-3-methylimidazolium dicyanamide ([EMIM][DCA]) ionic liquid for effective CO2/H2 separation, J. Membr. Sci. 597 (2020) 117623.

[29] A. Naderi, A. Asadi Tashvigh, T.-S. Chung, M. Weber, C. Maletzko, Molecular design of double crosslinked sulfonated polyphenylsulfone /polybenzimidazole blend membranes for an efficient hydrogen purification, J. Membr. Sci. 563 (2018) 726–733.

[30] X. Mei Wu, Q. Gen Zhang, P. Ju Lin, Y. Qu, A. Mei Zhu, Q. Lin Liu, Towards enhanced CO2 selectivity of the PIM-1 membrane by blending with polyethylene glycol, J. Membr. Sci. 493 (2015) 147–155.

[31] C.A. Scholes, Blended perfluoropolymer membranes for carbon dioxide separation by miscible and immiscible morphologies, J. Membr. Sci. 618 (2021) 118675.

[32] S. Zhao, J. Liao, D. Li, X. Wang, N. Li, Blending of compatible polymer of intrinsic microporosity (PIM-1) with Tröger's Base polymer for gas separation membranes, J. Membr. Sci. 566 (2018) 77–86.

[33] E.T. Fox, J.E.F. Weaver, W.A. Henderson, Tuning Binary Ionic Liquid Mixtures: Linking Alkyl Chain Length to Phase Behavior and Ionic Conductivity, J. Phys. Chem. C 116 (2012) 5270–5274.

[34] A.S.L. Gouveia, C.E.S. Bernardes, E.I. Lozinskaya, A.S. Shaplov, J.N. Canongia Lopes, I.M. Marrucho, Neat ionic liquids versus ionic liquid mixtures: a combination of experimental data and molecular simulation, PCCP 21 (2019) 23305–23309.

[35] G. Chatel, J.F.B. Pereira, V. Debbeti, H. Wang, R.D. Rogers, Mixing ionic liquids – "simple mixtures" or "double salts"? Green Chem. 16 (2014) 2051–2083.

[36] R. Vijayaraghavan, T. Oncsik, B. Mitschke, D.R. MacFarlane, Base-rich diamino protic ionic liquid mixtures for enhanced CO2 capture, Sep. Purif. Technol. 196 (2018) 27–31.

[37] A.S.L. Gouveia, L.C. Tomé, I.M. Marrucho, Towards the potential of cyano and amino acid-based ionic liquid mixtures for facilitated CO2 transport membranes, J. Membr. Sci. 510 (2016) 174–181.

[38] A.S.L. Gouveia, L.C. Tomé, E.I. Lozinskaya, A.S. Shaplov, Y.S. Vygodskii, I. M. Marrucho, Exploring the effect of fluorinated anions on the CO2/N2 separation of supported ionic liquid membranes, PCCP 19 (2017) 28876–28884.

[39] X. Ma, P. Kumar, N. Mittal, A. Khlyustova, P. Daoutidis, K.A. Mkhoyan, M. Tsapatsis, Zeolitic imidazolate framework membranes made by ligand-induced permselectivation, Science 361 (2018) 1008–1011.

[40] J.E. Bachman, Z.P. Smith, T. Li, T. Xu, J.R. Long, Enhanced ethylene separation and plasticization resistance in polymer membranes incorporating metal–organic framework nanocrystals, Nat. Mater. 15 (2016) 845–849.

[41] L. Lang, F. Banihashemi, J.B. James, J. Miao, J.Y.S. Lin, Enhancing selectivity of ZIF-8 membranes by short-duration postsynthetic ligand-exchange modification, J. Membr. Sci. 619 (2021) 118743.

[42] Q. Ma, K. Mo, S. Gao, Y. Xie, J. Wang, H. Jin, A. Feldhoff, S. Xu, J.Y.S. Lin, Y. Li, Ultrafast Semi-Solid Processing of Highly Durable ZIF-8 Membranes for Propylene/Propane Separation, Angew. Chem. Int. Ed. 59 (2020) 21909–21914.

[43] W. Qiu, L. Xu, Z. Liu, Y. Liu, P. Arab, M. Brayden, M. Martinez, J. Liu, A. Roy, W. J. Koros, Surprising olefin/paraffin separation performance recovery of highly aged carbon molecular sieve hollow fiber membranes by a super-hyperaging treatment, J. Membr. Sci. 620 (2021) 118701.

[44] N. Zhilyaeva, E. Mironova, M. Ermilova, N. Orekhova, M. Dyakova, N. Shevlyakova, V. Tverskoii, A. Yaroslavtsev, Facilitated transport of ethylene through the polyethylene-graft-sulfonated polystyrene membranes, Role Humid., Separat. & Purif. Technol. 195 (2018) 170–173.

[45] L.C. Tome, D. Mecerreyes, C.S.R. Freire, L.P.N. Rebelo, I.M. Marrucho, Polymeric ionic liquid membranes containing IL-Ag+ for ethylene/ethane separation via olefin-facilitated transport, J. Mater. Chem. A 2 (2014) 5631–5639.

[46] H. Dou, B. Jiang, X. Xiao, M. Xu, X. Tantai, B. Wang, Y. Sun, L. Zhang, Novel Protic Ionic Liquid Composite Membranes with Fast and Selective Gas Transport Nanochannels for Ethylene/Ethane Separation, ACS Appl. Mater. Interfaces 10 (2018) 13963–13974.

[47] Y. Sun, H. Bi, H. Dou, H. Yang, Z. Huang, B. Wang, R. Deng, L. Zhang, A Novel Copper(I)-Based Supported Ionic Liquid Membrane with High Permeability for Ethylene/Ethane Separation, Ind. Eng. Chem. Res. 56 (2017) 741–749.

[48] M. Fallanza, A. Ortiz, D. Gorri, I. Ortiz, Experimental study of the separation of propane/propylene mixtures by supported ionic liquid membranes containing Ag +–RTILs as carrier, Sep. Purif. Technol. 97 (2012) 83–89.

[49] B. Jiang, W. Tao, H. Dou, Y. Sun, X. Xiao, L. Zhang, N. Yang, A Novel Supported Liquid Membrane Based on Binary Metal Chloride Deep Eutectic Solvents for Ethylene/Ethane Separation, Ind. Eng. Chem. Res. 56 (2017) 15153–15162.

[50] M. Fallanza, A. Ortiz, D. Gorri, I. Ortiz, Polymer–ionic liquid composite membranes for propane/propylene separation by facilitated transport, J. Membr. Sci. 444 (2013) 164–172.

[51] R. Zarca, A.C.C. Campos, A. Ortiz, D. Gorri, I. Ortiz, Comprehensive study on PVDF-HFP/BMImBF4/AgBF4 membranes for propylene purification, J. Membr. Sci. 572 (2019) 255–261.

[52] H. Dou, B. Jiang, X. Xiao, M. Xu, B. Wang, L. Hao, Y. Sun, L. Zhang, Ultra-stable and cost-efficient protic ionic liquid based facilitated transport membranes for highly selective olefin/paraffin separation, J. Membr. Sci. 557 (2018) 76–86.

[53] Dou, Haozhen, Jiang, Bin, Xiao, Xiaoming, Xu, Mi, Tantai, Xiaowei, Novel Protic Ionic Liquid Composite Membranes with Fast and Selective Gas Transport Nanochannels for Ethylene/Ethane Separation, ACS applied materials & interfaces, (2018).

[54] R. Deng, Y. Sun, H. Bi, H. Dou, H. Yang, B. Wang, W. Tao, B. Jiang, Deep Eutectic Solvents As Tuning Media DissolvingCu+ Used in Facilitated Transport Supported Liquid Membranefor Ethylene/Ethane Separation, Energy Fuels 31 (2017) 11146–11155.

[55] T.A. Reine, R.B. Eldridge, Absorption equilibrium and kinetics for ethylene–ethane separation with a novel solvent, Ind. Eng. Chem. Res. 44 (2005) 7505–7510.

[56] J.H. Dymond, K.N. Marsh, R.C. Wilhoit, K.C. Wong, M.D. Frenkel, Virial coefficients of pure gases, (2002).

[57] G. Zarca, I. Ortiz, A. Urtiaga, Copper (I)-containing supported ionic liquid membranes for carbon monoxide/nitrogen separation, J. Membr. Sci. 438 (2013) 38–45.

[58] K. Huang, X.M. Zhang, Y.X. Li, Y.T. Wu, X.B. Hu, Facilitated separation of CO2 and SO2 through supported liquid membranes using carboxylate-based ionic liquids, J. Membr. Sci. 471 (2014) 227–236.

[59] M. Xu, C. Guo, H. Dou, Y. Zuo, Y. Sun, J. Zhang, W. Li, Tailoring the degradation and mechanical properties of poly (ε-caprolactone) incorporating functional ε-caprolactone-based copolymers, Polym. Chem. 10 (2019) 3786–3796.

[60] C. Carolino, D. Azevedo, O. Alfredo, G. Daniel, O. Inmaculada, A perspective of solutions for membrane instabilities in olefin/paraffin separations: A review, Industrial & Engineering Chemistry Research, (2018) acs.iecr.8b02013-.

[61] M. Rungta, C. Zhang, W.J. Koros, L. Xu, Membrane-based ethylene/ethane separation: The upper bound and beyond, AIChE J. 59 (2013) 3475–3489.